RSC Advances

ROYAL SOCIETY OF CHEMISTRY

www.rsc.org/advances

RSC Advances

ARTICLE

Received 00th January 20xx,
Accepted 00th January 20xx

DOI: 10.1039/x0xx00000x

www.rsc.org/

Effect of B_2O_3 addition on optical and structural properties of TiO_2 as a new blocking layer for multiple dye sensitive solar cell application (DSSC)

Wassila SAIDI,[a] Nasreddine HFAIDH,[a] Mohammed RASHEED,[b] Mihaela GIRTAN,[b] Adel MEGRICHE[a] and Mohamed EL MAAOUI[a]

TiO_2-B_2O_3 Sol gel thin films were prepared using titanium (IV) isopropoxide as a Ti source and boric acid (H_3BO_3) as B precursor. B_2O_3 doping was found to improve significantly the characteristics of TiO_2 films making them suitable to use as blocking TiO_2 layers into multiple dye sensitized solar cells. Study was performed using 0 to 20 Molar percent B_2O_3. The films were deposited on ordinary lime glass sheets by spincoating, dried and sintered at 500°C. B_2O_3 acted as a flux and glass forming oxide leading to amorphous vitreous layers having an average thickness of 50 nm. Films were transparent, adherent and perfectly continuous without any leakage current. X-ray diffraction measurements prove that the cristallinity decreases with Boron contents meaning that amorphous phase was favoured. Surface morphology was investigated by Atomic Force Microscopy (AFM). It shows that film surface became more and more smooth and roughness decreased with the increase of B_2O_3 content. The Eg Raman-active phonon mode at 145 cm^{-1} reveals the same arrangement of TiO_2 octahedral observed in anatase phase. The Lorentzian multipeak fitting including the wavenumber range from 120 to 180 cm^{-1} showed the emergence of a new mode at 152 cm^{-1} whose the mode intensity increased with Boron concentration, we attributed it to the presence of Boron. The influence of the B_2O_3 dopant on the optical properties was examined by UV-Visible spectroscopy and spectroscopic ellipsometry. Refractive index (n), extinction coefficient (k) and optical band gap (Eg) have been extracted by fitting Ellipsometric spectra with the double new amorphous model. Difference between the optical gap values obtained from UV-Visible spectra and those calculated by ellipsometry did not exceed 0.3 eV. Optical band gap increases from 3.4 to 3.9 eV by increasing Boron contents from 0 to 20%. The increase of Eg is expected to induce an enhance output ddp into dye-sensitized solar cell cells.

1. Introduction

Sol-gel technology is a convenient method to prepare thin glass coatings, especially for a variety of either ceramic or metallic surfaces. It remains the cheapest method compared to chemical vapor deposition, pulsed laser deposition and reactive sputtering technique. Sol gel method was used to deposit various metal oxide materials

[a] Université de Tunis El Manar, Faculté des sciences de Tunis, (UR11ES18) Laboratoire de chimie minérale appliquée
[b] Université d'Angers, laboratoire photonique (LPHIA), LUNAM - 2 Bd. Lavoisier, 49045, Angers, France.
DOI: 10.1039/x0xx00000x

such as SiO_2, [1] SnO_2, [2] ZrO_2, [3] ZnO [4] and TiO_2.[5] Recently, this process is used also to deposit perovskite compounds such as $BaTiO_3$.[6] Sol gel technology allows to contol microstructure and film thickness. Among the different oxides, TiO_2 is currently the most interesting. Anatase films are performing for many industrial applications particularly as photocatalyst for water, [7] air purification [8] and for self-cleaning surfaces.[9] Additionally; it has antibacterial properties due to its high oxidation activity and super hydrophilicity.[10] In dye-sensitized solar cell (DSSC) field, purpose of our study, TiO_2 was used since the first studies because of its high energy gap.[11] A standard DSSC is composed by a layer of transparent conducting oxide (TCO) made usually with a fluorine-doped tin-oxide (FTO) deposited on a glass substrate. Then a nanostructured layer of TiO_2 porous oxide on which the dye is adsorbed. The latter is full with liquid or solid electrolyte. At least there is the counter electrode. Various efforts have been made to improve DSSCs' efficiency such as changing TiO_2 particle morphologies [12] and adding an insulating layer situated between fluorine doped tin oxide (FTO) and the porous titanium oxide. This work is focused on the fabrication of such a layer named also «dense layer", or "blocking layer“ or “compact layer” whose role is to improve the adhesion of the nanoporous TiO_2 to FTO substrate, to avoid current leakage and to prevent electron recombination between TiO_2 and FTO. [13] Many works were devoted to this topic. They used different metal oxides such as SiO_2, [14] Al-doped ZnO [13] and TiO_2 [15] which remains the most used material for this purpose. TiO_2 compact layer was elaborated by pre-treatment of FTO with $TiCl_4$ on the transparent electrode, [16] RF and pulsed DC magnetron sputtering. [17]

In view of the desired aims, to obtaining a transparent, continuous and perfectly insulating layer, all methods are possible although the benefits and disadvantages depend on the discretion of each. The use of $TiCl_4$ is very difficult because of its high reactivity with and even with air humidity, so the $TiCl_4$ bottles fume on opening in air laboratory and a bulk white precipitate occurs when it goes in contact with insufficient dried solid surfaces. RF and magnetron sputtering need high vacuum installations and are costly especially if large surfaces are wanted.

In this work, we choose to use the sol gel technique which is simple and allows the control of thickness as well as the introduction of doping oxides. We propose also introduce B_2O_3 as doping oxide. B_2O_3 doped TiO_2 layers were studied in two references, the first deals with the use B_2O_3-TiO_2 layers to degrade organic pollutants under visible light radiations [18] and the second concerns the fabrication of the porous TiO_2 layer of DSSC cells [19] In fact, the presence of B_2O_3 into the compact layer is more justified than its presence into the porous layer. This oxide is commonly used as a fluxing agent into the fabrication of ceramic enamels and glasses.[20, 21] Its introduction into the blocking layer will lower the melting temperature and facilitate the napping of substrate area. The layer thickness will be decreased and the transparency and the adherence will be increased.

Many works reported the change of optical and physical properties induced by doping the TiO_2 layer. In general we note an improve of the overall energy conversion efficiency of the DSSC. **Sangwook Lee** studied Nb-doped TiO_2 as a new compact layer. As a result, the efficiency of the DSSC with Nb-doped TiO_2 and 80 nm thick enhanced by 4.1% compared to DSSC with undoped TiO_2.[22] Zn-doped TiO_2 blocking layer were also investigated by Thanh-Tung Duong, the increase of efficiency with 20-nm thick Zn doped-TiO_2 blocking layer showed was about 1.32%, compared to undoped TiO_2 (20 nm). [23] Doping induce also a change into the gap energy of TiO_2. **Suk In Noh** reported that F-doped TiO_2 compact layer show a band gap equal to 3.8 eV instead of 3.56 eV for undoped TiO_2 film. [24]

This work is focused on the synthesis of a compact TiO_2 layer which is adherent to glass substrate, transparent and homogeneous. We choose to use TiO_2 doped with up to 20% mol B_2O_3. This layer was deposited directly on glass substrate in order to separate the observed phenomena. Obviously, the presence of the transparent conducting oxide is necessary for further applications. However, there are now several possibilities to choice the conducting layer and the success of the concordance of the TiO_2 layer and the glass substrate will remain whatever the choice of the interlayer between them mainly because the fact this layer is extremely thin and chemically inert towards the adjacent compounds. In addition the conducting layer does not affect the optical properties of the doped TiO_2 layer but it may complicate the treatment of the results.

2. Experimental method

2.1. Preparation of B_2O_3-doped TiO_2 thin films

Boron-doped TiO_2 thin films were prepared by Sol Gel process spin coating method in three steps. The aim of the process is to produce a homogeneous solution containing TiO_2-B_2O_3 precursors. The first step is to prepare an alcoholic B_2O_3 solution (A solution) by dissolving 20 g of boric acid (H_3BO_3) in 100 g of methanol.

The second step is to obtain a homogeneous TiO_2 solution (B solution). This was achieved by mixing ethanol as solvent, acetic acid as a stabilizing agent and titanium isopropoxide as a precursor. The final dipping solution was got by mixing two volumes V_1 and V_2 from A and B solutions respectively. Study of the Boron effect was achieved using the TiO_2 solution doped with x % B. x is the atomic percent of the B ion and is defined as x = [B/ (Ti + B)]/ 100. x took the values 0, 5, 10, 15, and 20 %. Subsequently, different B_2O_3 solutions were added into TiO_2 under vigorous stirring. The resultant dip solution remains transparent after use.

The different films were deposited on glass substrates which are carefully cleaned by ultrasonic treatment with acetone, ethanol and dichloromethane each for 10 min.

The Boron-doped TiO_2 coatings were prepared by spin-coating method with fixed spin speed of 3000 rpm for 1 min. All films undergo a heat treatment begins by drying at 100 °C for 10 minutes and ends by annealing in furnace at 500 °C.

2.2. Characterization methods

The structure of the Boron-doped TiO_2 films was examined by X-ray diffraction using a Cu Kα radiation (1.5406 A) Bruker D8 Advance diffractometer. Raman spectroscopy was performed with a LabRam HR and T64 000 spectrometer. The Lorentzian fitting was performed using the Fityk software.

The surface morphology of the TiO_2-B_2O_3 thin films was carried out using an Auto Probe CP-Research AFM (Thermo-microscopes) with a lateral resolution of 5 nm. UV transmittance analyses were monitored by a near-infrared to ultraviolet Spectrophotometry (NIR-UV-VIS) PerkinElmer type in the wavelength range of 200–2250 nm. Ellipsometric spectra were recorded at room temperature using a phase modulated spectroscopic ellipsometer (PMSE) from JOBIN - YNON HORIBA model UVISELTM in the wavelength range of 190 - 2100 nm. The chosen configuration for the modulator and analyzer positions were M=0° and A= 45° respectively.

The values obtained for TiO_2-B_2O_3 film thicknesses were estimated by a profilometer VeecoTM Dektak 6M and confirmed by ellipsometry. The photoluminescence (PL) spectra was measured with an excitation (360 nm) source using a 1000 W Xe arc lamp coupled to a monochromator as excitation source at room temperature.

3. Results and discussion

3.1. Structural analysis

Fig.1 presents the XRD spectra of samples with different Boron doping concentrations. We observe for pure titanium oxide thin films a broad peak at 2θ = 25° (**fig.1a**). Owing to literature, this peak is attributed to anatase titanium oxide phase. The large width of this peak indicates a poor crystallization state. As the film thicknesses of all the samples are almost similar, the intensity of this peak decreases with increasing Boron contents which indicate that Boron dopant promotes the formation of an amorphous structure; this is caused by the better melting of TiO_2 films.

The Raman spectra of TiO_2 films with different B_2O_3 contents are revealed in **Fig.2.**

For pure TiO_2, only the peak at 145 cm^{-1} appeared with a very low intensity. This peak is attributed to Eg mode of anatase phase. [25-26] After doping, the intensity of this mode increased and other Raman peaks at 125, 197 and 639 cm^{-1} appeared.

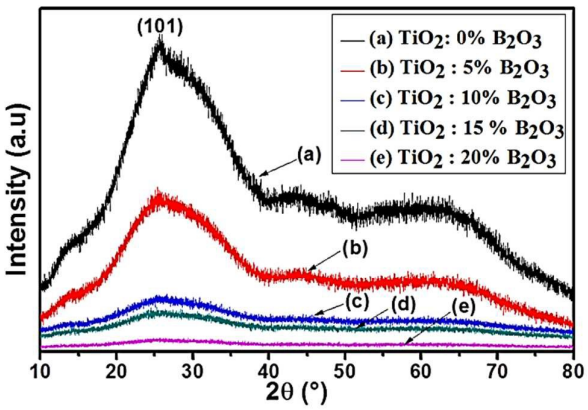

Fig.1 XRD patterns of TiO_2 films with different Boron contents

Owing to literature, they are attributed to Raman-active modes of anatase phase with the symmetries of 3Eg.[26]

In order to study the lattice vibrations, Lorentzian fittings of the Raman spectra for TiO_2 doped with 15 % (**fig.3a**) and 20% Boron (**fig.3b**) were performed into the wavenumber range from 120 to 180 cm^{-1}. Besides 2Eg modes of TiO_2 anatase (125 and 145 cm^{-1}), we show the emergence of a new peak at 152 cm^{-1}. It showed that the intensity of 2Eg modes respectively at 125 cm^{-1} and at 145 cm^{-1} decreased, while that of mode at 152 cm^{-1} increased with increasing of the boron amounts. The vibration mode at 152 cm^{-1} had not been described in literature; it is due to the presence of Boron dopant.

3.2. Morphologic analysis by Atomic Force Microscopy (AFM)

Boron doped TiO_2 films deposited on glass substrates were fully transparent to the naked eye. As shows in **fig.4**, Boron-TiO_2 thin films are characterized by a decrease in surface roughness with the increase of Boron dopant. The variation of the roughness and average grains size for the TiO_2 films as a function of Boron contents were plotted in **Fig.5.** The RMS values and the average grain size are 1.05 nm, 8.98 nm for pure TiO_2 films and 0.44 nm, 4.27 nm for the 20% B_2O_3-TiO_2 films respectively. The roughness fall indicates that the presence of Boron improves the homogeneity and the smoothness of the surface with small grain size.

3.3. UV transmittance analysis of TiO_2 thin films with various Boron dopant concentrations

Transmittance spectra of TiO_2 films doped with different Boron contents in the wavelength region from 200 to 800 nm are given in **fig.6.** Transmittance spectra revealed that the deposited thin films are transparent in visible region. They start absorbing in the range between 270 and 300 nm. After doping with Boron oxide (5%, 15%, 20%), there is a shift of the absorption threshold towards lower wavelengths.

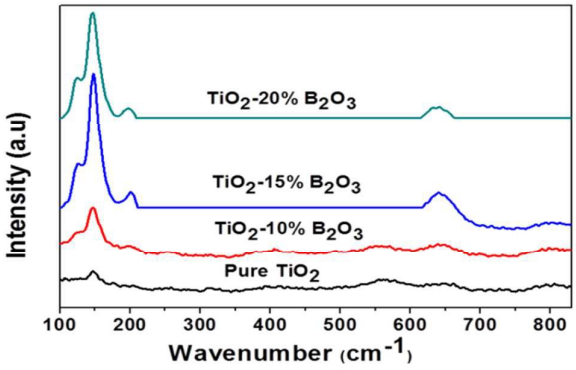

Fig.2. Raman spectra of TiO_2 films with different B contents

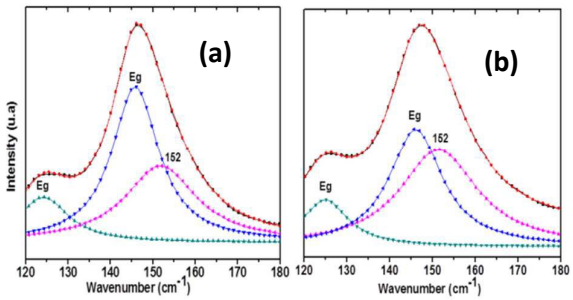

Fig.3. Lorentzian fittings of the spectra in the wavenumber range from 100 to 200 cm^{-1} for the TiO_2 films doped with (a) 15 % Boron and (b) 20% Boron.

The only exception is noted for TiO_2 film doped with 10% B_2O_3, there is a red shift of the absorption threshold. This result shows that doping affects the optical gap. Starting from transmittance spectra, we can determinate the optical band gap which is a prominent feature of TiO_2. The band gap values of all samples were obtained from the model proposed by Tauc,[27] where Eg related to the absorption coefficient by the following equation:

$$\alpha\, hv^n = A(hv - Eg)$$

Here α is the absorption coefficient, Eg is the absorption band gap, A is a constant depending on the transition probability, and n depends on the nature of transition. It is well known that TiO_2 possesses a direct and indirect band gap.[28] Most authors found that the anatase TiO_2 has only an indirect band gap, whereas rutile phase has a direct and an indirect band gap.[29] For an indirect band gap, the value of n is ½ while for the direct band gap, the value of n is 2.[30-31] In our case, XRD and Raman spectroscopy showed that anatase phase is the most probable.

The variation of $(\alpha hv)^{1/2}$ with photon energy is shown in **fig.7** for B_2O_3-doped TiO_2 films.

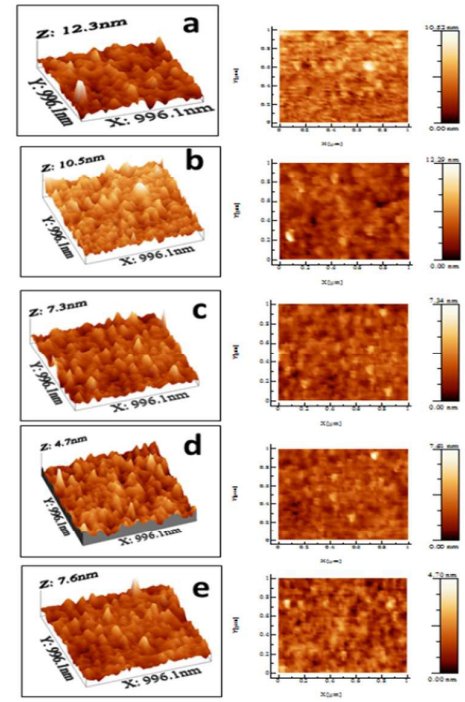

Fig.4. 2D and 3D Micrographs of TiO_2 single layer doped with (a) 0 %, (b) 5 %, (c) 150 %, (d) 15% and (e) 20 % B_2O_3

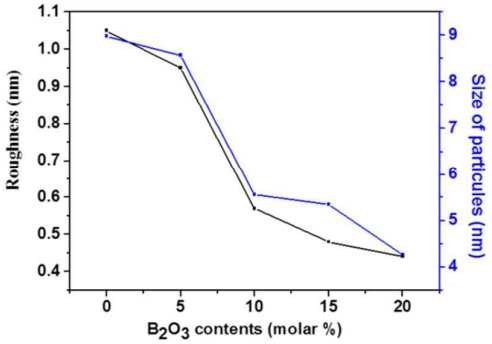

Fig.5 Roughness average and size particles of TiO_2 films as a function of Boron concentrations

The optical gap values were evaluated from the intercept of the linear portion of each curve hv in X-axis. The obtained values of TiO_2 thin films optical band gap are with the range reported in the literature of anatase form.[24,32] From **Fig.7**, it is clearly seen that the optical band gap is affected by Boron contents. Doping with 5%, 15% and 20% of B_2O_3 caused the TiO_2 optical band gap shift to higher energies. This result was earlier reported in another work on mesoporous TiO_2 modified by boron doping.[33] Adriana Zaleska has also found that the value of Eg increased from 3.29 eV (pure TiO_2) to 3.4 eV with 10% of boric acid.[34] This was explained by the increase of the

carrier concentration blocking the lowest states in the conduction band. This phenomenon is well known as the Burstein-Moss effect.[35] Gap values are similar to those obtained for F-doped TiO_2 blocking thin films in DSSC.[24] He deduced that a degenerated n-type TiO_2 layer between the substrate and the nanoporous TiO_2 layer was obtained to furnish an ohmic contact, leading to the enhanced performance of DSSCs by reducing interfacial resistance.[24]

The gap value of pure TiO_2 was 3.6 eV and it decreases to 3.56 eV after doping with 10% B_2O_3. This redshift for TiO_2 doped with 10% B_2O_3 was observed by some authors. They assumed that the red shift of the absorption edge is derived from the mixing of B 2p states and O 2p states.[36] It is noted that the 10% B_2O_3-TiO_2 film revealed the best photocatalytic activity both in visible and UV light.[37]

The values of the gap will be confirmed by ellipsometry spectroscopic.

3.4. Spectroscopic ellipsometry modeling and analysis

As it is known, Spectroscopic ellipsometry (SE) determines the complex reflectance ratio ρ defined in terms of the standard ellipsometric parameters Ψ and Δ:[38]

$$\boldsymbol{\rho = \frac{R_p}{R_s} = \tan\psi \exp(i\Delta)}$$

Where R_p and R_s are the reflection coefficients for light polarized parallel (p) and perpendicular (s) to the sample's plane of incidence respectively. It is an indirect technique, which requires an appropriate optical model to fit the experimental spectra with maximum accuracy. Ellipsometry allows to determinate the influence of Boron doping on the optical constants (n, k and Eg), and the thin films thickness of all samples. The best optical model adopted for B-doped TiO_2 semiconductor thin films consists of three layers: void / glass / TiO_2.

Fig.8 reveals a good agreement between experimental and theoretical spectrum achieved for B_2O_3-doped TiO_2 films. The good fit designates that the "Double new amorphous" dispersion formula describe perfectly the optical properties of B_2O_3-doped TiO_2 films.[39-40] Table 1 recapitulates the double new amorphous parameters used to analyse ellipsometry data obtained for TiO_2 films doped with different Boron contents. The refractive index (n) and the extinction coefficient (k) are definite as follows:

$$\mathbf{n(E) = \sqrt{\varepsilon_\infty} + \sum_{n-1}^{2} \frac{B0_n \,.\, E + C0_n}{E^2 - B_n \,.\, E\, C_n}}$$

$$\mathbf{(E) = \sum_{n-1}^{2} \frac{A_n\,(E - Eg)^2}{E^2 - B_n \,.\, E + C_n} \qquad E > Eg}$$

Where

$$B0_n = \frac{A_n}{Q_n}\left(-\frac{B_n^2}{2} + Eg\,.\,B_n - E_g^2 + C_n\right)$$

$$\mathbf{C0_n = \frac{A_n}{Q_n}\{(E_g^2 + C_n).\frac{B_n}{2} - 2.Eg.C_n\}}$$

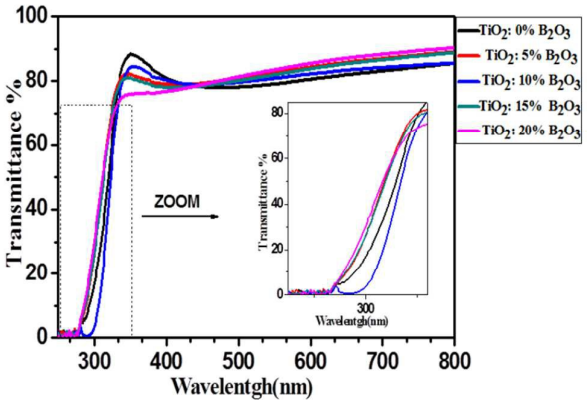

Fig.6 Transmittance spectra for TiO_2 thin films doped with different Boron contents

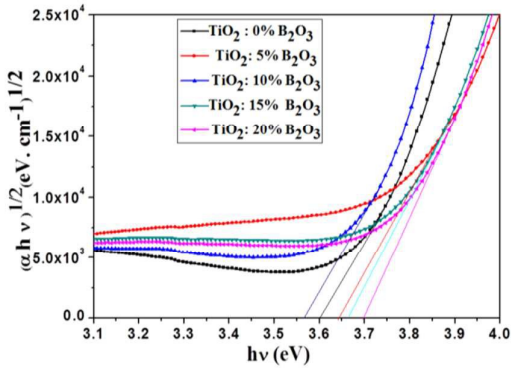

Fig.7 $(\alpha h\nu)^{1/2}$ versus the photon energy for TiO_2 thin films doped with different Boron contents

$$\mathbf{Q_n = \frac{1}{2}\sqrt{4\,C_n - B_n^2}}$$

The term ε∞: is an additional parameter corresponding to the high-frequency dielectric constant. It is at least superior to one and equal to the value of the dielectric function when ω → ∞.[41-44]

A, B, C: are positive non zero parameters referring to the electronic structure of the material. For parameters An, Bn, Cn, n refers to the number of oscillators in our case n=2 for double new amorphous and the parameters number is 8.

An (in eV): is related to the dipole matrix squared and gives the amplitude of the extinction coefficient peak.

Generally, 0 < An <2.

B_n /2 (in eV): is approximately the energy at which the extinction coefficient is maximum (peak of absorption). As the value of B increases, the absorption peak is shifted towards the UV region. Generally, 3 <B_n <30.

Cn (in eV2): is related to the broadening term of the absorption peak. It depends on the energy difference between different states and on the lifetime of transition.

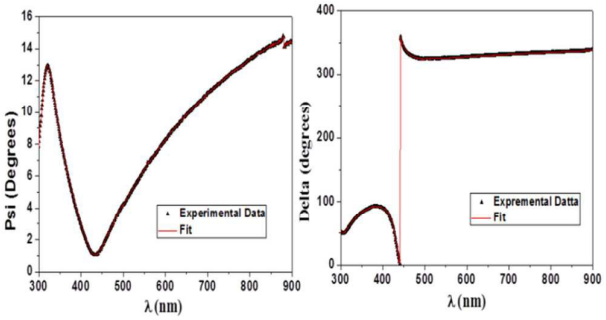

Fig.8. Typical ellipsometry spectra and best fit of TiO_2 doped with Boron of parameters (a) Δ and (b) ψ as functions of λ with "double new amorphous" dispersion formula

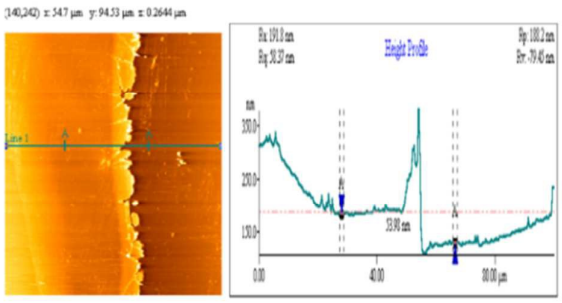

Fig.9. Cross section AFM image of TiO_2 thin film doped with 5% B_2O_3

Generally, 3< C_n <150.

3.4.1. Thickness, refractive index (n) and extinction coefficient (k)

Firstly, it must be noted that Ellipsometric measurements and optical parameters (n, k) of B_2O_3-doped TiO_2 thin films have not yet studied.

From table 1, it is seen that the thicknesses determined by the fitting are in good agreement with the result obtained by profilometer DEKTAK. **Fig.9** shows a cross section realized by AFM for TiO_2 doped with 5% B_2O_3. The thickness is equal to 53.98 nm by comparing it with that found by ellipsometry (53.2 nm). It was found that the film thickness corresponded with the profilometer and ellipsometry technique. We observe that difference between the values obtained by the three methods does not exceed 2 nm. Table.1 show that thickness values decrease slightly from 52 to 45 nm when the Boron contents increase from 0 to 20%. This slight decrease is due to the better melting of TiO_2 in presence of boron oxide, which was confirmed by the AFM. **Fig.10** shows the variation of refractive index (n) and extinction coefficient (k) respectively as a function of wavelength at different Boron contents, calculated from the extracted best-fitted parameters. Spectra showed a similar shape than cited in literature.[45-46] We note that n and k are considerably affected by Boron doping concentration. These optical factors increase with increasing of wavelength up to threshold with a maximum value that corresponds to the band gap. After doping with 10% B_2O_3, the maximum of n (n_{max}) undergoes a shift to the high wavelengths, but, for the remaining of samples (5%, 15% and 20% B_2O_3), this peak shifted to lower wavelengths. This result indicated the change of optical gap with doping, which is in good agreement with the results obtained by UV-Visible spectroscopy. **Fig.10b** demonstrates that all the samples have

Table 1 Parameter values of the double new amorphous model used for fitting the optical functions and the thickness of the TiO_2 thin films doped with different Boron contents

Parametrs	0% B	5% B	10% B	15% B	20% B
X^2	2.7	1.5	1.5	1.4	3.2
ε_∞	4.49	3.8	5.54	3.55	3.52
Eg (eV)	3.43	3.64	3.31	3.68	3.95
A_1	0.29	0.26	0.0002	0.001	1.38
B_1	7.70	6.47	8.49	5.76	5.70
C_1	17 .8	17.76	18.69	17.53	17.49
A_2	0.32	0.01	0.33	0. 18	0.14
B_2	8.62	8.25	8.76	7.68	6.86
C_2	19.27	17.52	21.4	14.78	13.49
Thickness by SE (nm)	52.09	51.16	55.34	50.42	45.80
Thickness by profilometer (nm)	55.3	53.2	58.7	50.6	47.3

dielectric thin films.[47] For all samples; values of refractive index are greater than 2. These higher values make this material suitable for antireflection coatings.[48] After 370 nm, refractive index described by a gradual decrease when the wavelength increases for each TiO_2 thin films inclosing various Boron doping. Moreover, the relation of Clausius Mossotti explained the correlation between the refractive index (n), the polarizability (αm) and the density (ρ) by the following equation:

$$\frac{n^2-1}{n^2-2} = \frac{4\Pi N_a}{3\,M}\ \alpha_m\ \rho$$

Where N_a is Avogadro's constant and M is the molecular weight. The density of different films was calculated from the values of the refractive index at 550 nm. As seen in **Fig.11b**, Refractive index (n_{550}) and density values are 2.31, 0.92 cm^3 for pure TiO_2 films and 2.12, 0.82 cm^3 for 20% B_2O_3-TiO_2 films respectively. It is clearly seen in **Fig.11a** that refractive index decreases when boron contents increase from 0 to 20 %. Obtained n_{550} values are in good agreement with literature

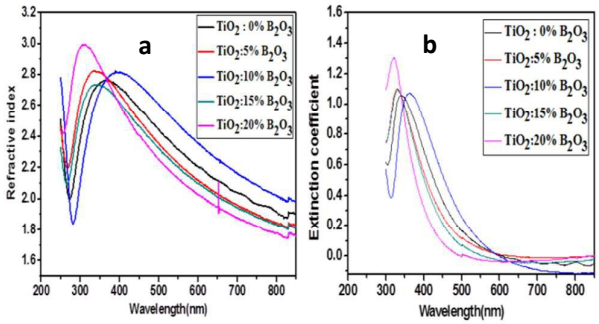

Fig.10. the calculated refractive index spectra (a), extinction coefficient spectra (b) of TiO_2 thin films with different B_2O_3 contents, based on the results of the double new amorphous model fitting

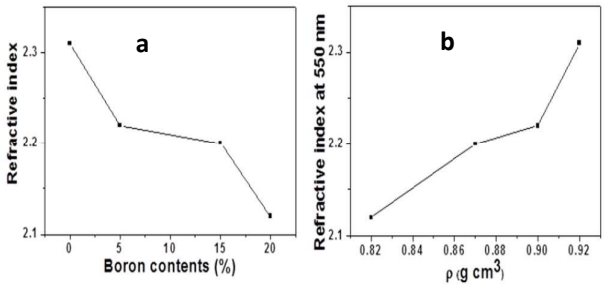

Fig.11. The variation of refractive index of TiO_2 thin films (a) with various B- doped concentrations at 550 nm and (b) as function of density.

values of anatase TiO_2 films.[26] This result confirms that the decrease in refractive index is actually due to the decrease of density. Correspondingly, the value of the refractive index of our samples is smaller than the ones characteristic for the anatase phase; which is reported to be approximately 2.5. Several authors attributed the low values of the refractive index to the lack of cristallinity.[39, 49] XRD results confirmed the low of cristallinity for TiO2-B_2O_3 films.

3.4.2. Discussion of the optical band gap values obtained by UV-Visible spectroscopy and that by Ellipsometry

As shown in **Table.2**, Optical band gap values obtained both by ellipsometry and by UV-Visible spectroscopy are nearby to literature values.[50] Ellipsometry reveals that optical band-gap energy progressively increases from 3.4 eV to 3.95 eV with the increase of the Boron concentration from 0% to 20%. We note an exception for 10% B_2O_3 where the gap decreases.

This evolution is in accordance with the findings acquired by UV-Visible spectroscopy. It was demonstrated that the increment of band gap for the TiO_2-B_2O_3 (5%, 15% and 20%) is due to the Burstein-Moss effect.[48] With widening Boron doping, Fermi level shifts into the conduction band of the TiO_2-B_2O_3 films. Since, the donor electrons occupied the states underneath Fermi level, optical transitions can only occur between the valence band and the states above Fermi level in the conduction band, which results in the increment of the optical gap.[50] It is difficult to select which of two methods is more accurate. In reality each of two methods postures an accuracy problem.

In the UV-visible spectroscopy case, plotting the tangent to the curve $(\alpha h\nu)_n = f(h\nu)$ can easily induce errors. For ellipsometry, calculating Eg uses parameters that cannot be with accuracy. In our case we found a difference of 0.3 eV which is not always in the same case.

3.5. Photoluminescence (PL)

Table 2 Gap values for TiO_2 thin films doped with different Boron contents

% B_2O_3	Gap by Ellipsometry (eV)	Gap by UV-Vis spectroscopy(eV)
0	3.34	3.6
5	3.68	3.64
10	3.31	3.56
15	3.69	3.66
20	3.95	3.70

Photoluminescence spectroscopy is employed to examine the electronic structure, the photo generated electron-hole pairs in semiconductors and the rate of recombination. The room temperature PL spectra obtained under excitation at 360 nm for TiO_2 thin films with different B_2O_3 concentrations (0-20 %). **Fig.11.a** shows that all PL emission peaks are observed at about 544 nm and another smaller peak at 485 nm. The two peaks were attributed to the transitions from oxygen vacancies with one-trapped electrons and two-trapped electron to valence band of TiO_2 respectively.[51]

The corresponding emission peaks are respectively 2.28 and 2.56 eV. This indicates that the position of the energy levels associated with the two types of oxygen vacancies is respectively at 0.8 and 0.44 eV beneath the conduction band of TiO_2 respectively.[51] Several factors can affect the PL intensity. **Shuai Chen** shows that the decrease of PL intensity is related to the better cristallinity. [52] This finding is in good agreement with our results. As we have defined the values of the optical gap by ellipsometry, we note in **fig.11.a** that quenching or enhancement intensity PL is related to the gap values. A high intensity was obtained for gap value of about 3.9 eV for TiO_2 doped with 20% B_2O_3, whereas a low intensity is observed for the low optical gap of about 3.31 eV for TiO_2 doped with 10% B_2O_3. Thus, it appears that doping of TiO_2 with

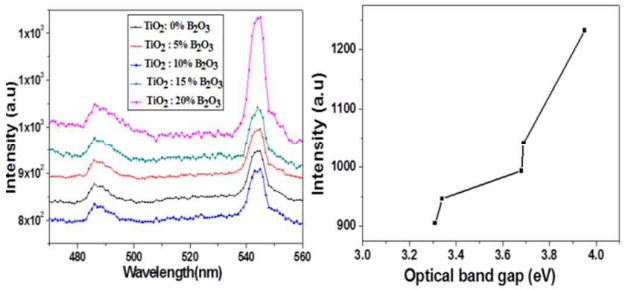

Fig.12. Room-temperature PL emission spectra of TiO_2 film doped with different Boron contents (a) and variation of PL intensity as a function of optical band gap of Boron-doped TiO_2 films (b).

boron has abundant influence on the band gap and the defect emissions of the top TiO_2 films.[53]

Conclusions

B_2O_3-doped TiO_2 thin films have been prepared by sol-gel method and the coatings were annealed at 500 °C. Results indicate that the addition of Boron dopant affected structural and optical properties of TiO_2 thin films. The cristallinity of TiO_2 thin films decreased when the boron oxide content increased from 0 to 20 % explained by the flux effect of B_2O_3. The Raman spectra show that the Eg Raman-active phonon modes appeared at 145 cm^{-1}, 199, 638 cm^{-1} justified the presence of anatase phase. The absorption edge of TiO_2 films shifted towards lower wavelengths from 370 to 309 nm with the increase of Boron contents. Extinction coefficient and refractive index are affected by boron oxide content. As demonstrated by UV-Visible spectroscopy and the spectroscopic ellipsometry, the band gap energy of TiO_2 thin films increases from 3.4 to 3.9 eV when the Boron contents increase from 0 to 20%. The room temperature PL spectra suggest that the emission intensities increase with increasing Boron contents. It is showed that the positions peaks are situated at about 2.28 and 2.56 eV. These are assigned to the transitions from oxygen vacancies with one-trapped electrons and two-trapped electron to valence band of TiO_2 respectively. The present results will be helpful for future applications of TiO_2-based semiconductor devices, especially, as a blocking layer in multiple dye solar cells application, to prevent the back electron transfer and resulted in the reduced interfacial resistance.

Acknowledgements

This work was realized in collaboration between the photonics laboratory (LPHIA) from Angers, France and the Laboratory of applied Mineral chemistry (UR11ES18), Tunisia.

The authors acknowledge and thank Miss Emmna Kadri from applied physics laboratory faculty of science Sfax, Tunisia for her help in the AFM observations and for the photoluminescence measurements.

Notes and references

1 Hsieh. Tung. Li, Chu. Ann. Kuo, Huang. Wen. Yao, *J. Nanosci. Nanotechno*, 2013, **13**, 279-287.
2 M. Marikkannan, V. Vishnukanthan, A. Vijayshankar, J. Mayandi, and J. M. Pearce, *Aip. Adv*, 2015, **5**, 027122.
3 S. Seidel, A. Sabelfeld, R. Strohmeyer, G. Schreiber, V. Klemm, D. Rafaja, Y. Joseph, J. Heitmann*, Thin Solid Films*, 2016, **606**, 13–18.
4 T. Demes, C. Ternon, D. Riassetto, H. Roussel, L. Rapenne, *I. Gélard, C. Jimenez, V. Stambouli, M. Langlet, J. Phys. Chem. Solids,* 2016, **95**, 43–55**.**
5 G. Kenanakis, D. Vernardoua, A. Dalamagkas, N. Katsarakis, *Catalysis. Today*, 2015, **240**, 146–152.
6 Ling Huang, Ying Dai n , Hua Xiao, Xinmei Pei, Wen Chen, *Ceram. Int*, 2016, **42**, 9046–9050.
7 E. Boonen, and A. Beeldens, *J. Coat*, 2014, **4**, 553-573.
8 D. Mardare, A. Yildiz, M. Girtan, A. Manole, M. Dobromir, M. Irimia, C. Adomnitei and N. Cornei, *J. Appl. Phys*, 2012, **112**, 073502.
9 S. R. Meher and L. Balakrishnan, *J. Mater. Sci. Semicond. Process*, 2014, **26**, 251–258.
10 Sung Min Kim, Insik In and Sung Young Park, *Surf. Coat. Technol*, 2016, **294**, 75–82.
11 Ladislav. Kavan and Michael Gratzel, *electochimica acta*, 1995, **40**, 64-652.
12 Jeganathan Akilavasan, Maufick Al-Jassim, and Jayasundera Bandaraa, *J. Nanophotonics*, 2015, **9**.
13 Ding-Yeng Chen, Jin-Yih Kao, Chun-Yao Hsu, Che-Hsiung Tsai, *J. Electroanal. Chem*, 2016, 766, 1–7.
14 Liangliang Liang, Yumin Liu and Xing-Zhong Zhao, *Chem. Commun*, 2013, **49**, 3958—3960.
15 Yanhui Chen, Hongzhou Zhang, Dniel Fox, Colm C. Faulkner, David Jeng, Mazhar Bari, *Mater. Sci. Eng B*, 2013, 71– 76.
16 N. G. Park, G. Schlichthörl, J. van de Lagemaat, H. M. Cheong, A. Mascarenhas and A. J. Frank, *J. Phys. Chem. B*, 1999, **103**, 3308-3314.
17 17 [Q.Q. Liu, D.W. Zhang, J. Shen a , Z.Q. Li, J.H. Shi, Y.W. Chen, Z. Sun, Z. Yang and S.M. Huang, *Surf. Coat. Technol*, 2013, **231**, 126–130.
18 X. Lu, B. Tian, F. Chen and J. Zhang, *Thin Solid Films***,** 2010**,** 519**, 111–116.**
19 H. Tian, L. Hu, C. Zhang, S. Chen, J. Sheng, L. Mo, W. Liua and S. Dai , *J. Mater. Chem*, 2011, **21**, 863–868**.**
20 Charles R. Kurkjian, William R. Prindle, *J. Am. Ceram.* Soc, 1998, **81**, 795–813.
21 Xiaodong Wang, Guangming Wu, Bin Zhou and Jun Shen, 2013, *Mater. J*, **6**, 2819-2830.
22 Sangwook Lee, Jun Hong Noh, Hyun Soo Han, Dong Kyun Yim, Dong Hoe Kim, Jung-Kun Lee, Jin Young Kim, Hyun Suk Jung, and Kug Sun Hong, *J. Phys. Chem. C,* 2009, **113**, 6878–6882.
23 Thanh-Tung Duong, Hyung-Jin Choi, Soon-Gil Yoon, *J. Alloys. Compd*, 2014, **591**, 1–5.
24 Suk In Noh, Kokn-Nara Bae, Hyo-Jin Ahn, Tae-Yeon Seong, *Ceram. Int*, 2013, **39**, 8097–8101.
25 M. C. Kao, H. Z. Chen, S. L. Young, C. Y. Kung and C. C. Linc, *Thin Solid Films*, 2009, **517**, 5096–5099.
26 W. F. Zhang, M. S. Zhang, Z. Yin and Q. Chen, *J. Appl. Phys. B*, 2000, **70**, 261–265.

27 J. Tauc, R. Grigorovici and A. Vancu, *J. Phys. Stat. Sol*, 1966, **15**, 627.
28 K. H. Leong, H. Y. Chu, S. Ibrahim and P. Saravanan, *Beilstein. J. Nanotechnol*, 2015, **6**, 428–437.
29 S. Valencia, J. M. Marín and G. Restrepo, *Open. Mater. Sci. J*, 2010, 4, 9-14.
30 S. J. Darzi, A. R. Mahjoub and A. Nilchi, *J. Physica E*, 2009, **42**, 176–181.
31 Zhao, Y. Li, C. Liu, X. Gu, F. Jiang, H. Shao, W. Zhang and L. He, Y, *J. Mater. Lett*, 2007, **61**, 79–83.
32 Paweł Karasin ski, Ewa Gondek, Sabina Drewniak, Anita Kajzer, Natalia Waczyn ska-Niemiec, Marcin Basiaga, Weronika Izydorczyk and Youssef E.L. Kouari, *Opt. Mater*, 2016, **56**, 64–70.
33 M. A. Islam, M. J. Haither, I. Khan and M. Islam, *J. Electr. Electron. Eng*, 2012, **3**, 18-24.
34 H. Tian, L. Hu, Ch. Zhang, S. Chen, J. Sheng, L. Mo, W. Liua and S. Dai, *J. Mater. Chem*, 2011, **21**, 863–868.
35 A. Zaleska , J. W. Sobczak, E. Grabowska and J. Hupka, *Appl. Catal, B*, 2008, **78**, 92–100.
36 W. Zhao, W. Ma, C. Chen, J. Zhao and Z. Shuai, *J. Am. Chem. Soc*, 2004, **126**, 4782–4783.
37 Xiaona Lu, Baozhu Tian, Feng Chen and Jinlong Zhang, *Thin Solid Films*, 2010, **519**, 111–116.
38 R. Oommen, P. U. Rajalakshmi and S. Sudha, *Int. J. Appl .Phys. Math*, 2012, **2**, 439-441.
39 H. G. Tompkins and E. A. Irene, Handbook of Ellipsometry, Springer-Verlag, 2005.
40 A.V. Manole, M. Dobromir, M. Girtan, R. Mallet, G. Rusu and D. Luca, *J. Ceram. Int*, 2013, **39**, 4771–4776.
41 E. D. Palik, Handbook of Optical Constants of Solids II, Chap. 7.
42 A. R. Forouhi and I. Bloomer, *Phys. Rev. B*, 1986, **34**, 7018-7026.
43 A. R. Forouhi and I. Bloomer, *Phys. Rev. B*, 1988, **38**, 1865.
44 N. Bsiri, M.A. Zrir, A. Bardaoui and M. Bouaïcha, *J. Ceram. Int*, 2016, **42**, 10599–10607.
45 D. Saha, R.S. Ajimsha, K. Rajiv, C. Mukherjee, M. Gupta, P. Misra and L.M. Kukreja, *Appl. Surf. Sci*, 2014, **315**, 116–123.
46 C. M. Maghanga, G. A. Niklasson and C. G. Granqvist, *Thin sold films*, 2009, **518**, 1254-1258.
47 A. Dakka, J. Lafait, C. Sella, S. Berthier, M. Abd-Lefdil, J. C. Martin and M. Maaza, *J. Appl. Opt*, 2000, **39**, 2745-2753.
48 D. Saha, R. S. Ajimshaa, K. Rajiv, C. Mukherjee, M. Gupta, P. Misra and L. M. Kukreja, *J. Appl. Surf. Sci*, 2014, **315**, 116–123.
49 W. Chiappim , G.E. Testoni , R.S. Moraes, R.S. Pessoa , J.C. Sagas, F.D. Origo, L. Vieira and H.S. Maciel, *Vacuum*, 2016, **123**, 91-102.
50 Q. H. Lia, D. Zhua, W. Liua, Y. Liuc and X. C. Ma, *J. Appl. Surf. Sci*, 2008, **254**, 2922–2926.
51 Jixiang Yuan, Enjun Wang, Yongmei Chen, Wensheng Yang, Jianghong Yao and Yaan Cao, *Appl. Surf. Sci*, 2011, **257**, 7335–7342.
52 Shuai Chen, Xiaoru Zhao, Haiyan Xie, Jinming Liu, Libing Duan, Xiaojun Ba, Jianlin Zhao, Appl. Surf. Sci, 2012, **258**, 3255– 3259.
53 X. D. Zhou, X. H. Xiao, J. X. Xu, G. X. Cai, F. Ren and C. Z. Jiang, *Lett. J. expl. Phys*, 2011, **93**, 57009.